Department of Chemistry

Atomic Layer Deposition of Thermoelectric ZnO Thin Films

Tommi Tynell

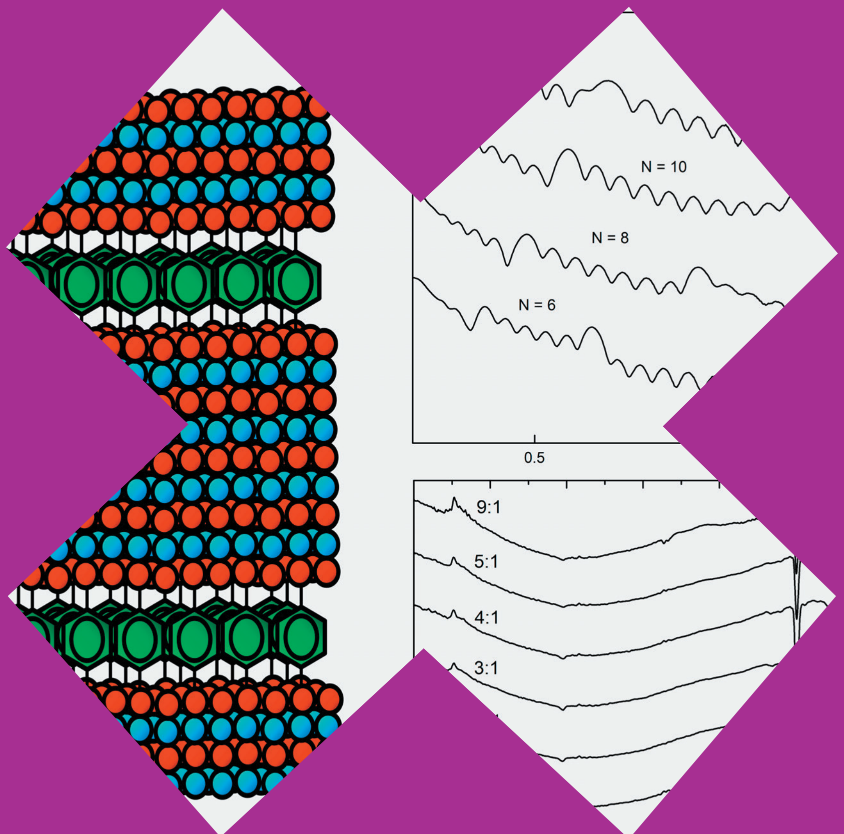

Aalto University

DOCTORAL
DISSERTATIONS

Aalto University publication series
DOCTORAL DISSERTATIONS 194/2013

Atomic Layer Deposition of Thermoelectric ZnO Thin Films

Tommi Tynell

A doctoral dissertation completed for the degree of Doctor of Science (Technology) to be defended, with the permission of the Aalto University School of Chemical Technology, at a public examination held at the lecture hall Ke2 of the school on 13 December 2013 at 12.

Aalto University
School of Chemical Technology
Department of Chemistry
Laboratory of Inorganic Chemistry

Supervising professor
Academy Professor Maarit Karppinen

Thesis advisor
Prof. Hisao Yamauchi

Preliminary examiners
Prof. Mato Knez, Ikerbasque Nanoscience Cooperative Research Center, Spain
Prof. Väinö Sammelselg, University of Tartu, Estonia

Opponent
Prof. Julien Bachmann, Friedrich-Alexander-Universität Erlangen-Nürnberg, Germany

Aalto University publication series
DOCTORAL DISSERTATIONS 194/2013

© Tommi Tynell

ISBN 978-952-60-5452-0
ISBN 978-952-60-5453-7 (pdf)
ISSN-L 1799-4934
ISSN 1799-4934 (printed)
ISSN 1799-4942 (pdf)
http://urn.fi/URN:ISBN:978-952-60-5453-7

Unigrafia Oy
Helsinki 2013

Finland

Aalto University

Abstract

Aalto University, P.O. Box 11000, FI-00076 Aalto www.aalto.fi

Author
Tommi Tynell

Name of the doctoral dissertation
Atomic Layer Deposition of Thermoelectric ZnO Thin Films

Publisher School of Chemical Technology

Unit Department of Chemistry

Series Aalto University publication series DOCTORAL DISSERTATIONS 194/2013

Field of research Inorganic Chemistry

Manuscript submitted 2 September 2013 **Date of the defence** 13 December 2013

Permission to publish granted (date) 6 November 2013 **Language** English

☐ **Monograph** ☒ **Article dissertation (summary + original articles)**

Abstract

Thermoelectric energy harvesters hold great potential for reducing our dependence on conventional energy sources by making use of untapped heat sources and converting them into electricity. For the technology to be able to make a significant impact though, more efficient materials need to be developed. This is a huge challenge because of the interdependence of the physical properties that affect the performance of a thermoelectric material, and nanostructuring might be the only way to overcome this obstacle. This thesis presents research on the effect of inorganic dopants and inorganic-organic hybrid superlattice structures on the thermoelectric properties of ZnO thin films. Atomic layer deposition (ALD) was used to fabricate the thin films in this study due to the suitability of the technique for the deposition of precisely controlled nanostructures.

Zinc oxide is one of the most promising thermoelectric oxide materials, especially when doped with for instance Al or Ga, but it is somewhat held back by the lack of a stable p-type ZnO material. The effects of aluminum and phosphorus doping on the thermoelectric properties of ALD-grown ZnO thin films were investigated in this work, and both were found to increase the carrier concentration of ZnO, with Al turning out to be the better dopant in terms of improving thermoelectric performance. An attempt was also made to induce p-type conductivity in ZnO through thermal treatment of the P-doped films, but a deterioration of the electrical properties of the films was observed instead.

The fabrication of superlattice structures of organic layers within ZnO with a combination of the atomic and molecular layer deposition (MLD) techniques was successfully demonstrated for three different organic precursors: hydroquinone, 4-aminophenol and 4,4'-oxydianiline. All of the organic molecules were found to have an effect on the electrical and thermoelectric properties of ZnO, the magnitude of which varied noticeably between the different organic constituents despite their relatively similar structures. The observed effects from the introduction of the hybrid superlattice structures amounted to only small changes in the thermoelectric power factor of ZnO, and these changes were not cumulative with the effects of Al doping when hybrid superlattices were combined with Al doping. The net effect from the organic layers on the thermoelectric performance of ZnO is predicted to be greater than implied by the slight changes in power factor due to the expected decrease in thermal conductivity resulting from phonon inhibition by the organic layers.

Keywords ZnO, thermoelectricity, atomic layer deposition, thin film

ISBN (printed) 978-952-60-5452-0 **ISBN (pdf)** 978-952-60-5453-7

ISSN-L 1799-4934 **ISSN (printed)** 1799-4934 **ISSN (pdf)** 1799-4942

Location of publisher Helsinki **Location of printing** Helsinki **Year** 2013

Pages 123 **urn** http://urn.fi/URN:ISBN:978-952-60-5453-7

A? Aalto-yliopisto

Aalto-yliopisto, PL 11000, 00076 Aalto www.aalto.fi

Tiivistelmä

Tekijä
Tommi Tynell

Väitöskirjan nimi
Termosähköisten ZnO-ohutkalvojen atomikerroskasvatus

Julkaisija Kemian tekniikan korkeakoulu

Yksikkö Kemian laitos

Sarja Aalto University publication series DOCTORAL DISSERTATIONS 194/2013

Tutkimusala Epäorgaaninen kemia

Käsikirjoituksen pvm 02.09.2013 **Väitöspäivä** 13.12.2013

Julkaisuluvan myöntämispäivä 06.11.2013 **Kieli** Englanti

☐ **Monografia** ☒ **Yhdistelmäväitöskirja (yhteenveto-osa + erillisartikkelit)**

Tiivistelmä

Termosähköisellä energialouhinnalla on mahdollisuus vähentää riippuvuuttamme perinteisistä energialähteistä käyttämällä hyväksi hyödyntämättömiä hukkalämmön lähteitä ja muuttamalla ne sähköksi. Jotta teknologialla voisi olla merkittävä vaikutus, täytyy kuitenkin kehittää tehokkaampia termosähköisiä materiaaleja. Tämä on valtava haaste, sillä fysikaaliset ominaisuudet, jotka vaikuttavat materiaalin termosähköiseen suorituskykyyn, eivät ole toisistaan riippumattomia. Nanostrukturointi saattaa olla ainoa keino tämän ongelman ratkaisemiseksi. Tässä väitöskirjatutkimuksessa selvitettiin epäorgaanisten substituenttien ja hybridi-superhilarakenteiden vaikutusta ZnO-ohutkalvojen termosähköisiin ominaisuuksiin. Ohutkalvojen syntetisointiin käytettiin atomikerroskasvatusta (ALD), sillä menetelmä sopii ainutlaatuisen hyvin tarkasti kontrolloitujen nanorakenteiden valmistukseen.

Sinkkioksidi on yksi lupaavimmista termosähköisistä oksidimateriaaleista, erityisesti kun siihen on lisätty alumiinia tai galliumia, mutta stabiilin p-tyypin ZnO-materiaalin puuttuminen haittaa hieman sen käytettävyyttä. Alumiini- ja fosfori-substituenttien vaikutusta ALD:llä kasvatetun ZnO:n termosähköisiin ominaisuuksiin tutkittiin tässä työssä, ja molempien substituenttien havaittiin kasvattavan ZnO:n varauskuljettajatiheyttä, tosin alumiini osoittautui paremmaksi termosähköisen suorituskyvyn parantamisen kannalta. ZnO:n johtavuutta yritettiin myös muuttaa p-tyyppiseksi fosforia sisältävien ohutkalvojen lämpökäsittelyn avulla, mutta p-tyypin johtavuuden sijaan materiaalin sähköisten ominaisuuksien havaittiin heikkenevän huomattavasti.

Hybridi-superhilarakenteita valmistettiin onnistuneesti yhdistämällä atomikerroskasvatusta ja mokyylikerroskasvatusta (MLD), ja superhilarakenteiden muodostuminen osoitettiin kolmella eri orgaanisella lähtöaineella: hydrokinoni, 4-aminofenoli ja 4,4’-oksidianiliini. Kaikkien kokeiltujen orgaanisten molekyylien havaittiin vaikuttavan ZnO:n termosähköisiin ominaisuuksiin. Vaikutusten suuruus vaihteli lähtöaineesta riippuen, huolimatta siitä että lähtöaineiden rakenteet olivat melko samanlaiset. Hybridi-superhilojen vaikutukset johtivat vain pieniin muutoksiin ZnO:n termosähköisessä suorituskyvyssä, eivätkä muutokset olleet kumulatiivisia alumiini-substituenttien vaikutusten kanssa. Orgaanisten kerrosten aiheuttama parannus ZnO:n termosähköiseen suorituskykyyn uskotaan olevan suurempi kuin mittausten perusteella voi nähdä, sillä orgaanisten kerrosten odotetaan häiritsevän fononien liikettä ja siten johtavan lämmönjohtavuuden vähenemiseen.

Avainsanat ZnO, termosähköisyys, atomikerroskasvatus, ohutkalvo

ISBN (painettu) 978-952-60-5452-0 **ISBN (pdf)** 978-952-60-5453-7

ISSN-L 1799-4934 **ISSN (painettu)** 1799-4934 **ISSN (pdf)** 1799-4942

Julkaisupaikka Helsinki **Painopaikka** Helsinki **Vuosi** 2013

Sivumäärä 123 **urn** http://urn.fi/URN:ISBN:978-952-60-5453-7

Preface

The work presented in this thesis was carried out in the Laboratory of Inorganic chemistry at Aalto University School of Chemical Technology as well as in the Laboratory of Condensed-Matter Physics of Functional Materials at Nagoya University between November 2009 and August 2013. Tekes, Academy of Finland, the Scandinavia-Japan Sasakawa Foundation, the Research Foundation of Helsinki University of Technology, Fortum Foundation and the Finnish Chemical Society are gratefully acknowledged for financial support of this work.

First of all, I would like to thank my supervisor, Academy Professor Maarit Karppinen, for giving me an opportunity to pursue doctoral studies in the Laboratory of Inorganic Chemistry and for providing me with guidance and encouragement throughout the years. Her support was especially appreciated during the last year of my doctoral studies, where it was instrumental in enabling me to meet all the deadlines. Her wide international connections also made it possible to enrich my studies with a highly beneficial research period at Nagoya University.

I would also like to express my gratitude to Professor Hisao Yamauchi for many inspiring conversations and for providing insights into the world of physics. I am grateful to Professor Ichiro Terasaki for agreeing to host me in his research group at Nagoya University and especially for the many valuable discussions and lessons during that time that made the visit a truly enlightening experience. The support and guidance of everyone in Prof. Terasaki's group, especially Assistant Professor Ryuji Okazaki, was also greatly appreciated; it ensured that my stay in Nagoya was a productive one. I also wish to thank Dr. Soichiro Shibasaki for his patient instructions on the measurement of thermoelectric properties during his visits to Aalto University.

I would like to thank all the researchers, staff and faculty members of the Laboratory of Inorganic Chemistry for their support in my research and for providing a wonderful environment for doing research. I am especially grateful to Dr. Jari Malm for introducing me to the intricacies of ALD research, to Mrs. Pia Sundberg for the many occasions where she helped me with measurements and to Dr. Markus Valkeapää for guidance with the various XRD methods necessary for my research. A special thank you goes out to Ms. Outi Parkkima and Mr. Sami Vasala for their company and

support during this journey, which already started years before our doctoral studies.

Most of all, I would like to thank my parents for their support and always making it easy to follow whatever path in life I desired. I also want to thank my brother and all the guys from the “Lahela Roleplayers” for many lasting memories and for making sure I always had a place to unwind. Of the many friends who were there during my studies at the old TKK I would like to especially thank Petri for his friendship and the guys of TLT Productions who truly made it the time of my life.

Tommi Tynell

Espoo, November 2013

Contents

List of Publications i
The Author's Contribution ii
List of Abbreviations and Symbols iii

1. Introduction 1
2. Thermoelectric Materials 4
   2.1 Seebeck Effect 4
   2.2 Thermoelectric Figure of Merit 5
   2.3 State-of-the-Art Thermoelectric Materials 6
   2.4 Nanostructuring 7
3. Thermoelectric Properties of ZnO 8
   3.1 Bulk ZnO 8
   3.2 ZnO Thin Films 9
4. Experimental Procedures 11
   4.1 Atomic and Molecular Layer Deposition 11
   4.2 ALD of ZnO 13
   4.3 ALD Reactors 14
   4.4 X-Ray Reflectivity 15
   4.5 Optical Measurements 17
   4.6 Thermoelectric Property Measurements 18
5. Doping of ZnO Thin Films with Al and P 20
   5.1 Chemical Composition and Structure 20
   5.2 Thermoelectric Properties 23
6. ZnO-Organic Superlattice Structures 25
   6.1 Characterization of the Organic Layers 26
   6.2 Thermoelectric Properties 28
   6.3 Hybrid Superlattices of Al-doped ZnO 30
7. Conclusions 34

References 36

List of Publications

In addition to the present review, this thesis consists of the following publications (**I–VI**), which are referred to in the text by their corresponding Roman numerals. The original publications are found in Appendices **I–VI**.

I T. Tynell and M. Karppinen, Atomic layer deposition of ZnO: a review, *Semiconductor Science and Technology*, *Submitted Manuscript*.

II T. Tynell, R. Okazaki, I. Terasaki, H. Yamauchi and M. Karppinen, Electron doping of ALD-grown ZnO thin films through Al and P substitutions, *Journal of Materials Science* **48** (2013) 2806-2811.

III T. Tynell, R. Okazaki, I. Terasaki, H. Yamauchi and M. Karppinen, Atomic layer deposition of Al-doped ZnO thin films, *Journal of Vacuum Science and Technology A* **31** (2013) 01A109.

IV T. Tynell and M. Karppinen, ZnO:hydroquinone superlattice structures fabricated by ALD/MLD, *Thin Solid Films*, *In Press*.

V T. Tynell, I. Terasaki, H. Yamauchi and M. Karppinen, Thermoelectric characteristics of (Zn,Al)O / hydroquinone superlattices, *Journal of Materials Chemistry A* **1** (2013) 13619-13624.

VI T. Tynell, H. Yamauchi and M. Karppinen, Hybrid inorganic-organic superlattice structures with atomic layer deposition/molecular layer deposition, *Journal of Vacuum Science and Technology A*, *In Press*.

The Author's Contribution

Publication **I** The author researched the relevant literature on the review topic. The author had a major role in writing the manuscript.

Publication **II** The author defined the research plan together with the co-authors and did all the experimental work. The results were interpreted together with the co-authors. The author had a major role in writing the manuscript.

Publication **III** The author defined the research plan together with the co-authors and did all the experimental work. The results were interpreted together with the co-authors. The author had a major role in writing the manuscript.

Publication **IV** The author defined the research plan together with the co-authors and did all the experimental work. The results were interpreted together with the co-authors. The author had a major role in writing the manuscript.

Publication **V** The author defined the research plan together with the co-authors and did all the experimental work. The results were interpreted together with the co-authors. The author had a major role in writing the manuscript.

Publication **VI** The author defined the research plan together with the co-authors and did all the experimental work. The results were interpreted together with the co-authors. The author had a major role in writing the manuscript.

List of Abbreviations and Symbols

ALD	atomic layer deposition
AP	4-aminophenol
DEZ	diethyl zinc
DMZ	dimethyl zinc
FTIR	Fourier transform infrared spectroscopy
GIXRD	grazing incidence X-ray diffraction
GPC	growth per cycle
HQ	hydroquinone
IR	infrared
MLD	molecular layer deposition
ODA	4,4'-oxydianiline
RTA	rapid thermal annealing
TMA	trimethyl aluminum
TMP	trimethyl phosphate
UV	ultraviolet
XRF	X-ray fluorescence
XRR	X-ray reflectivity

e	electron charge
ε_∞	high-frequency permittivity
κ	thermal conductivity
L	Lorentz number
m^*	effective mass
n	charge carrier concentration
ρ	electrical resistivity
S	Seebeck coefficient
σ	electrical conductivity
T	temperature
ω_p	plasma frequency
Z	thermoelectric figure of merit
ZT	dimensionless figure of merit

1. Introduction

As the world is facing ever increasing demands for energy, the importance of meeting those demands in a sustainable way is growing larger all the time. Various renewable forms of energy production have enjoyed substantial progress technologically and economically during the last decade, but much still needs to be done to ensure that our energy infrastructure can stay on a sustainable footing. This cannot be achieved through one technological solution alone, but rather requires the utilization of a number of energy production technologies and measures to improve energy efficiency.

Energy harvesting is a term used for a number of technologies that utilize ambient energy sources or waste energy and convert them into electricity to power a variety of wireless applications. Examples of energy harvesting technologies include photovoltaics (converting light into electricity), piezoelectric devices (capable of generating electricity from mechanical strain) and thermoelectric generators, which can convert waste heat into electricity. These methods of energy harvesting could, if employed on a large scale, lessen the burden of conventional energy production systems by improving energy efficiency in existing applications or even through the use of concentrated energy harvesters for power generation. Photovoltaics have already reached a level of wide-spread applicability, but of the other energy harvesting technologies thermoelectricity has the best potential to significantly improve the state of our energy use and production.

Thermoelectric generators are capable of using any sort of heat source, from low-temperature sources like the human body to high-temperature industrial processes, to generate electricity. This opens up a huge reserve of untapped energy in the form of waste heat that can be utilized for useful purposes. Since waste heat forms by far the largest part of our energy losses at every stage of the energy supply chain, from generation to transmission to end-use, the conversion of even a small part of this heat back into usable electricity could lead to large reductions in our energy use. Thermoelectric generators do not have any moving parts, making them extremely robust and reliable, and they can be easily scaled up or down to fit applications of

all sizes. However, the use of these generators has been held back by the low conversion efficiency that can be achieved with state-of-the-art thermoelectric materials, making many potential applications for the technology economically unviable. Therefore, the development of better thermoelectric materials is a must for realizing the full potential offered by the technology.

The challenges involved in improving the performance of thermoelectric materials, unfortunately, are formidable. Because the main physical properties affecting the performance of thermoelectric materials usually cannot be independently controlled, novel materials design approaches are needed in order to circumvent, to some extent at least, the physical limitations of the materials. This has led to the use of a number of materials with complex structures from skutterudites[1] to clathrates[2] and layered oxide materials,[3,4] but the approach with the most potential is nanostructuring, where the material is controlled at the nanometer scale to create structures with unusual physical properties.[5-9]

In addition to performance, there are other factors to consider when choosing materials for a thermoelectric generator such as price, toxicity, environmental impact and availability that make the choice of materials somewhat complicated. Another factor is the temperature range where a generator is to be used, because thermoelectric materials typically perform better as the temperature gets higher. Current state-of-the-art thermoelectric materials are heavily based on tellurium compounds,[10,11] which raises concerns about the availability of tellurium should thermoelectric energy harvesting become truly widespread.

Oxides are a relatively new class of materials to be investigated for their thermoelectric properties. Their performance does not yet quite match that of the more traditional materials used, but their advantage is in their generally excellent raw material availability, low price, non-toxicity and capability of withstanding higher temperatures.[4,12] Zinc oxide is one of the more promising thermoelectric oxides due to the very high thermoelectric figure of merit measured for its cation-doped variants at 1000 °C.[13-15] With further improvements that could be achieved with nanostructuring techniques, ZnO's performance could be improved further and it could be made applicable at lower temperatures as well.

Atomic layer deposition (ALD) is a chemical thin-film deposition technique that can offer excellent control over the deposition process, enabling the fabrication of high-quality, conformal thin films with precisely determined structures and thicknesses. It is ideal for the fabrication of layered nanostructures, because the self-limiting nature of the ALD reactions enables the deposition of even single layers of a material on a

variety of substrate shapes and sizes.[16,17] Another feature of the technique is the possibility of depositing entire molecules instead of atoms, in which case another name for the technique is usually used: molecular layer deposition (MLD). By combining ALD and MLD, it is possible to deposit thin films of hybrid materials consisting of alternating layers of inorganic and organic materials.[18] These hybrid materials have the potential to combine properties of inorganic and organic materials in novel ways, creating new combinations of properties that can be used in applications such as transparent conductors, gas-permeation barriers and thin-film transistors.

This thesis presents work done with the objective of investigating and improving the thermoelectric properties of ZnO thin films using the ALD technique. The main aim of the study was to determine the effects of inorganic dopants and organic layers on these properties and compare their effectiveness. The existing research on the deposition of ZnO with ALD was extensively reviewed.[I] The influence of the deposition temperature during the ALD process and the effects of two different cation dopants, aluminum and phosphorus, on ZnO's thermoelectric properties were investigated.[II,III] Three different organic molecules, hydroquinone, 1,4-aminophenol and oxydianiline, were used in conjunction with the ZnO ALD process to fabricate hybrid thin films and the consequent formation of hybrid superlattice structures was demonstrated.[IV,VI] The effects of co-doping ZnO with both inorganic and organic layers was also investigated and found to hold potential benefits for the material's thermoelectric performance.[V]

2. Thermoelectric Materials

The thermoelectric effect describes the direct conversion processes between thermal and electrical energy, and consists of three closely related physical phenomena: the Seebeck effect, the Peltier effect and the Thomson effect. The Seebeck effect describes the generation of electricity from a temperature gradient, while the Peltier effect details the creation of a temperature gradient with electric current, and the Thomson effect defines the generation of heat in a current-carrying conductor where a temperature gradient is present. The Seebeck effect is the basis of thermocouples and can also be used for small-scale electricity generation, and the Peltier effect can be used to construct solid-state cooling and heating devices. Some of the advantages of using thermoelectric materials in these applications include their very good scalability and durability due to the lack of moving parts, but their biggest disadvantage is their often very low efficiency, for which better thermoelectric materials need to be developed.

All materials can be thought to have some thermoelectric character (albeit in most cases very weak), but generally the term is only used for the best materials. There is a variety of different material and structure types that can lead to good thermoelectric properties, but all the best thermoelectric materials can be classified as semiconducting due to the fact that they have a carrier concentration in the optimal range for maximizing a material's thermoelectric performance.[6,19]

2.1 Seebeck Effect

The Seebeck effect is a physical process whereby a voltage is generated between two ends of a thermoelectric material when a temperature gradient is applied over it. This electromotive force causes the movement of charge carriers from the hot end to the cold, and the direction of the corresponding electric current depends on the type of charge carrier that is dominant in the material. Therefore, by combining n-type and p-type thermoelectric materials in an appropriate way it is possible to construct an electric circuit.

An illustration of a typical setup for using thermoelectric materials to exploit a heat source is presented in Figure 1.

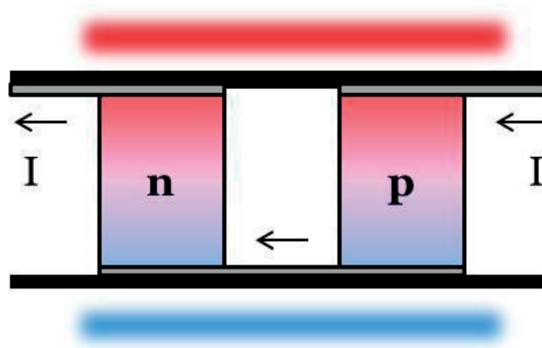

Figure 1 A setup for using two thermoelectric materials to generate a current from a heat source.

The design in Figure 1 is the most common way to construct a thermoelectric harvester; this way the n and p "legs" are connected parallel to each other in terms of the temperature gradient but in series in terms of the electric circuit. Any number of these pairs can be connected to create a device that takes full advantage of any temperature gradient over it.

2.2 Thermoelectric Figure of Merit

The magnitude of the Seebeck effect in a given material is described with the Seebeck coefficient, *S*, which is defined as the generated voltage difference per degree of temperature difference and is usually given in μV/K. When evaluating the potential of a thermoelectric material, it is customary to use the figure of merit, *Z*, which is defined according to the following equation:

$$Z = \frac{\sigma S^2}{\kappa} \tag{1}$$

where σ is the electrical conductivity and κ is the thermal conductivity of the material. The rationale behind the definition is the desire to have a material where the current can flow easily (high electrical conductivity) and where the temperature gradient can be maintained as large as possible (low thermal conductivity). Often the figure of merit is multiplied with the temperature to get the dimensionless *ZT* value. The best thermoelectric materials have *ZT* values of over 1 and the very best have reached 2, but the majority of materials still have values well below those levels.[6,19,20]

Another term that is often used when comparing thermoelectric materials is the power factor, which is defined as the top part of Equation (1), i.e. σS^2.

The reason for using the power factor instead of *ZT* is that often it is very challenging to measure thermal conductivity reliably, so the power factor presents a simpler, albeit less accurate, standard for comparing thermoelectric materials.

Improving the figure of merit outlined in Equation 1 is challenging because the terms in the equation are not completely independent of one another. For one, they are all directly related to the charge carrier concentration of the material, but while a large carrier concentration will lead to high electrical and thermal conductivities, it will also reduce the Seebeck coefficient. Therefore, a compromise has to be made between the parameters, meaning that semiconductors have the optimal carrier concentration for maximizing *ZT*.

A common strategy for improving thermoelectric performance has been to try and reduce the thermal conductivity of the material and specifically the lattice thermal conductivity, κ_L. The Wiedemann-Franz law states that electrical and thermal conductivity due to electrons are inextricably linked through the following relation:

$$\frac{\kappa_e}{\sigma} = LT \tag{2}$$

where L is the Lorentz number, 2.44×10^{-8} WΩK^{-2}. This means that the effect of any changes in the electronic thermal conductivity on the *ZT* value will be offset by a corresponding change in electrical conductivity. The lattice thermal conductivity, though, is free from such constraints and minimizing it is a good way to improve *ZT*. This has led to the introduction of a number of complex structures such as skutterudites and half-Heusler compounds where the intricate lattice contributes to the reduction of thermal conductivity.[1,6,19,20]

2.3 State-of-the-Art Thermoelectric Materials

By far the most commonly used thermoelectric materials are Bi_2Te_3 and Sb_2Te_3, along with a number of other telluride compounds. Alloys of Bi_2Te_3 and Sb_2Te_3 are capable of reaching a *ZT* value of 1 at temperatures up to 200 °C, and at higher temperatures tellurides such as PbTe and alloys of Te, Ag, Ge and Sb (the so-called TAGS) form some of the best performing materials. As well as these tellurium materials perform though, their *ZT* values are still not high enough for the widespread adoption of thermoelectric modules in a variety of applications, so other material groups have emerged with the potential to surpass the performance of tellurides.[6,19,20]

Many of the more researched thermoelectric materials can be classified as skutterudites or clathrates, which are structures with voids in them, into which doping cations can be inserted. These cations have quite a lot of room to move and can therefore "rattle" within the structure, acting as a phonon scattering center and decreasing the thermal conductivity of the material. Examples of these types of materials include materials based on $CoSb_3$ and various complex structures based on Si, Ge or Sn.[6,19,20]

Oxide materials generally cannot match the *ZT* values of the aforementioned materials, but they have a number of other advantages that make up for that deficiency, such as abundance of raw materials, non-toxicity and the ability to withstand very high temperatures. The most researched oxide materials are Na_xCoO_2, $Ca_3Co_4O_9$ and ZnO, which have reached *ZT* values of 0.6-1.2.[4,6,19,20]

2.4 Nanostructuring

While great improvements in *ZT* have been achieved with conventional materials design approaches, there is a limit to how far they can go, so many research efforts have turned to nanostructuring in order to achieve even greater improvements in thermoelectric performance. There are many benefits to fabricating nanostructured versions of thermoelectric materials, which can range from nanoscale particles[7,9,21-23] to superlattice structures consisting of extremely thin layers of one material within thicker layers of another and even 1- and 0-dimensional structures.[9, 24-26] When electrons are constrained to such low dimensions, the distribution of their density of states changes in a way that could theoretically lead to huge improvements in the material's Seebeck coefficient.[5,27-30] Another effect from nano-structuring is the reduction of thermal conductivity from either the increased number of grain boundaries or from the variation of the material layers in a superlattice.[31,32] In this case the dimensions of the particles or layers can be made shorter than the mean free path of phonons so that their propagation is inhibited without affecting electron transport too much.

3. Thermoelectric Properties of ZnO

Zinc oxide is a semiconductor with a number of useful properties that have made it a subject of intensive research in recent decades. The high transparency of ZnO to visible light combined with its tunable electrical conductivity enable its use in applications ranging from thin film transistors to the buffer layers of solar cells. ZnO's direct band gap of 3.37 eV at room temperature also means that it can be used in optoelectronic applications in the near-UV spectral range, including light-emitting diodes and photodetectors. Due to its piezoelectric properties, ZnO is also used in applications such as micro-electromechanical systems and sensors for detecting chemicals or gases. ZnO has also turned out to be one of the most promising thermoelectric oxide materials, especially at high temperatures.[33-35]

Zinc oxide crystallizes in the hexagonal wurtzite structure and displays an intrinsic n-type conductivity which was originally attributed to oxygen vacancies and Zn interstitials formed during the synthesis process, but has since been shown to be caused by other unintentional impurities incorporated into the material during synthesis.[36-38] Partly because of the strong n-type character of undoped ZnO, it has proven difficult to induce p-type conductivity in the material through the introduction of acceptor impurities. There are several reports of p-type conductivity achieved in ZnO by doping it with for instance P or N,[39-41] but the reproducibility and durability of this p-type doping are still problematic. Moreover, the thermoelectric performance of p-type ZnO has not been determined as of yet. The lack of p-type ZnO materials is hindering the applicability of ZnO in thermoelectric modules and p-n junctions, so a solution to the p-type doping problem is one of the major challenges of ZnO research.

3.1 Bulk ZnO

The thermoelectric properties of bulk ZnO have been the subject of a lot of research since the potential of Al-doped ZnO was discovered in the 1990's,

when a *ZT* value of 0.3 was observed for the material at 1000 °C.[13,14] This value has since been improved even further, and the current highest value stands at 0.65; achieved by co-doping ZnO with 2 at.% each of Ga and Al.[15] Alloys of ZnO and In_2O_3 are another group of materials that have often been studied for their thermoelectric properties, although they do not match the performance achieved with Al doping.[42-46] Further improvement in ZnO's properties through doping, however, seems difficult, so the way to raise ZnO's *ZT* to a new record will necessarily include some sort of nanostructuring approaches. In fact, it has already been demonstrated that fabricating nanocomposites out of Al-doped ZnO can significantly improve the material's figure of merit.[47]

The lack of a p-type ZnO material hurts its applicability in thermoelectric applications, because it is always desirable to construct the n and p legs of a thermoelectric module out of variants of the same material if possible. This will minimize potential problems arising from different material properties such as the thermal expansion coefficient and could also simplify the production process. Unfortunately the reliable fabrication of p-type ZnO materials is challenging, and there are no reports on the thermoelectric properties of p-type ZnO.

3.2 ZnO Thin Films

Thin films of ZnO have also been investigated for their thermoelectric properties as early as 1979,[48] but the efforts to improve them really started in the 1990's. Similarly to bulk ZnO, Al,[49-52] In,[53-55] Ga[56-58] and various combinations of them[59-62] are common dopants that have been used to improve the thermoelectric performance of ZnO thin films. The values obtained for thin film samples are in the same range as those for bulk samples, although it is hard to compare their performance directly because thermal conductivity is seldom reported for the thin film samples due to the difficulties in setting up a reliable measurement. Therefore, the comparison typically has to be made with just the power factor. There is one study[63] that reports a thermal conductivity value almost a magnitude lower than the bulk value for Al-doped ZnO, illustrating the potential of thin films in improving ZnO's thermoelectric figure of merit.

Nanostructuring is also the logical next step in improving thermoelectric thin films, perhaps more so than with bulk samples, and they are especially suited for the fabrication of superlattice structures. Alloys of In_2O_3 and ZnO (also called In-doped ZnO) spontaneously form superlattice structures under the right conditions and mixing ratios, and their thermoelectric properties have been reported for both thin films[59,62] and bulk samples.[46]

There is also a report on the patterning of layers consisting of ZnO and Ga-doped ZnO,[64] but overall these types of nano- or microstructured thin films remain relatively unexplored in the context of ZnO's thermoelectric properties.

4. Experimental Procedures

The objective of the research presented in this thesis was the investigation and possible improvement of the thermoelectric properties of ALD-grown ZnO thin films through the introduction of inorganic and organic dopants. To achieve this, an extensive series of ZnO thin films with aluminum or phosphorus doping or hybrid superlattice structures were deposited on silicon and borosilicate glass substrates using two different reactor designs. Analysis of the samples was mainly performed on the glass-deposited samples, but Si substrates were used for infrared spectroscopy and X-ray fluorescence measurements.

Analysis of the samples included grazing incidence X-ray diffraction (GIXRD) and X-ray reflectivity (XRR) for determining the structure of the samples, Fourier transfer infrared (FTIR) spectroscopy and X-ray fluorescence (XRF) for analyzing the chemical composition of the films and low-temperature Seebeck coefficient and resistivity measurements for determining the thermoelectric properties. Some of the used equipment and related methodology are discussed in this chapter.

4.1 Atomic and Molecular Layer Deposition

Atomic layer deposition (ALD) is a thin film deposition technique based on sequential surface reactions of gas-phase reagents that are introduced into the reactor one at a time. The self-limiting nature of the reactions ensures that only a single atomic layer is deposited at a time, enabling precise control of the layer structure and thickness of the deposited films through simple process design. Other advantages offered by ALD include the generally very good quality of the resultant films and conformality on even very high-aspect-ratio surfaces, as long as the process is designed so as to provide enough time for the reactants to diffuse to all the available surface sites. These properties have led to the adoption of ALD in a variety of technological applications, most prominently the microelectronics industry,

where ALD is playing a key role in enabling the fabrication of ever smaller material layers for electronic chips.

Molecular layer deposition (MLD) is the name given to a variant of ALD where the aim is to deposit layers of entire organic molecules instead of single atomic layers. While organometallic compounds are often used as ALD precursors, they are designed to react with the film surface and other precursors in a way that leaves nothing of the organic part in the deposited film. In the case of MLD the organic precursors are designed to be deposited in their entirety, either reacting with other organic molecules to create a fully organic thin film or with conventional ALD precursors to create hybrid inorganic-organic films. The deposition of hybrid thin films with a combination of ALD and MLD is particularly exciting, as it can be used to create a huge variety of different structures with potentially unique combinations of material properties.[65-74] There are a number of applications that have been proposed for such hybrid thin films, from gas permeation barriers to flexible conductors, and their potential for thermoelectric materials has also been noted.[75] In particular, the high control over the layer structure offered by both ALD and MLD can be exploited to create hybrid superlattices or nanolaminates with potentially large improvements in their thermoelectric properties over the inorganic parent phase.

There are many factors to consider when designing an ALD process, from reactor design to pulse and purge times, but the most important ones are the choice of precursors and precursor/deposition temperatures. Liquid precursors with high vapor pressures are optimal, typically requiring no heating and only short pulsing times, but in many cases solid precursors have to be used. In that case, the precursor needs to sublimate in vacuum at a reasonably low temperature and the required pulsing times are generally longer. In all cases, though, the precursors determine the range of deposition temperatures by their reactivity and thermal stability. If the temperature is too low, the precursors might not have enough energy to react or could even condensate on the substrate. If the temperature is too high, the precursors could start to break down and deposit unwanted compounds on the substrates or already deposited layers might sublimate away. All these temperature-dependent processes are reflected in the rate of growth of the thin film, which is usually expressed as growth per cycle (GPC), i.e. the thickness of a layer that is deposited by one ALD cycle, which consists of single pulses of each of the precursors required for the target compound separated by inert gas purges. Therefore, for most ALD processes there is a temperature range, commonly referred to as the ALD window, where none of the above deleterious effects take place and consequently the GPC value stays more or less constant. It is usually

desirable to find the ALD window for a given process and perform the depositions within that range, but good quality films can usually be obtained outside the ALD window as well if the application requires it. There might even be benefits to performing depositions outside the ALD window such as the possibility to tune the electrical properties of the film via the introduction of impurities into it.

4.2 ALD of ZnO

An ALD process for ZnO was developed pretty early on, and there are a number of possible precursors that can be used in ALD ZnO process, but by far the most common Zn precursor used in ALD is diethyl zinc (DEZ) which reacts readily with H_2O through the following mechanism:

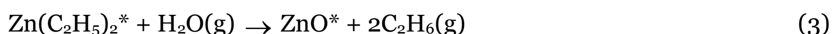

$$Zn(C_2H_5)_2^* + H_2O(g) \rightarrow ZnO^* + 2C_2H_6(g) \quad (3)$$

The reaction of DEZ with water is quite exothermic and can be used to deposit ZnO thin films even at room temperature. Typical deposition temperatures for DEZ-based ZnO deposition processes are in the range of 100 – 200 °C, but the DEZ precursor has been successfully used at temperatures as high as 600 °C.[76-78]

Dimethyl zinc (DMZ), which bears a close resemblance to DEZ, reacts in a similar way with H_2O and can be used in more or less the same range of deposition temperatures, although the ALD window is generally reported at slightly lower temperatures for DMZ. In a study investigating the effect of the Zn precursor choice on the properties of ZnO thin films, it was found that DMZ results in a slightly higher growth rate compared to DEZ, and the orientation of the resultant ZnO thin films is also different, but otherwise DMZ and DEZ produce ZnO films of equal quality.[79]

The ALD window for a typical ZnO ALD process using DEZ and H2O as precursors can be estimated to be around 110 – 170 °C. The growth per cycle (GPC), i.e. the thickness of the layer deposited by a single ALD cycle consisting of pulses of the zinc and oxygen precursors separated by purging steps, for a DEZ/H2O process within this window is around 1.8 – 2.0 Å/cycle, although there is a lot of variation in the reported GPC values due to the effects from the reactor design and other process parameters such as the pulsing and purging times. The interplanar distances in the hexagonal unit cell of ZnO range from 2.48 Å for the (101) planes to 2.60 Å and 2.82 Å for the (002) and (100) planes,[77] respectively, so the typical growth rates for ZnO within the ALD window are close to the ideal monolayer growth values.

ALD-grown ZnO crystallizes in the hexagonal wurtzite structure, and a high degree of crystallinity is usually obtained in the as-deposited films even when using relatively low deposition temperatures. The structure of the films can be controlled somewhat through the deposition temperature, which has been observed to affect the preferred orientation of the grains in ZnO films,[80-82] but apart from that the process parameters and precursors have little effect on the structural properties of the ZnO films. However, the deposition temperature does have an effect on the stoichiometry of the ZnO structure, which has a large effect on the electrical properties of the films. Because the intrinsic n-type conductivity of ZnO originates from the presence of defects and impurities in the ZnO crystal, its electrical properties can be controlled to some extent by controlling the amount of these defects and impurities. In ALD processes this is most easily achieved by controlling the deposition temperature, since it directly influences the reactivity of the precursors on the film surface and thus can have an effect on the stoichiometry of the film. The influence of the deposition temperature on the electrical properties of ALD-grown ZnO is seen in the increase of the films' conductivity with increasing deposition temperature, although at very high temperatures the films' resistivity will start to increase again. The minimum values for ZnO film resistivity are typically achieved with deposition temperatures of 180 – 250 °C. In this temperature range resistivity values in the 10^{-3} Ωcm range have been achieved.[83]

4.3 ALD Reactors

There were two designs of ALD reactors used in this work for the depositions: an R-100 reactor from Picosun and an F-120 from ASM Microchemistry. Although they work under the same principles, the design of the two reactors is quite different. Pictures of the two reactors are presented in Figure 2. The main difference of the reactors is in the delivery of the precursors, particularly when using solid precursors. In the F-120 reactor, there are eight gas lines leading into the reactor chamber and there is a constant flow of nitrogen gas through the lines, which is offset by the main N_2 flow in the reactor. Solid precursor chemicals are placed into small "boats" within these gas lines, heated to its sublimation temperature with heating elements and pulsed into the reactor by increasing the flow of N_2 through the line. In the R-100 reactor, there are similar gas lines leading into the reactor chamber, but instead of placing the precursors inside the lines, they are in separate containers that are connected to the gas lines through valves. This design difference along with the larger size of the precursor container and a different placement of the thermocouple leads to

differences in the precursor temperature required to achieve a sufficient vapor pressure for pulsing significant reactant amounts into the reactor. In practice, it was found that the R-100 reactor required significantly higher settings for the precursor temperature to ensure steady film growth.

Figure 2 The two ALD reactors used in this study: the F-120 reactor on the left and the R-100 reactor on the right.

In addition to the different precursor temperatures, there was also a slight difference observed in the properties of thin films deposited at the same temperatures in different reactors. This was not entirely surprising, since the electrical properties of ZnO thin films are very sensitive to the deposition temperature, and judging from the quite different ALD window temperature ranges reported for ALD ZnO processes, the design of the reactor also plays a role here. For the most part, though, the reactors produced comparable thin films of generally very good quality with only occasional small gradients observed in film thicknesses.

4.4 X-Ray Reflectivity

The X-ray reflectivity (XRR) measurement technique was used to analyze the thicknesses of the samples. The technique is based on X-ray diffraction measurements in the $\theta/2\theta$ configuration, but using very low angles. The X-ray beams reflected and refracted by a thin film and its underlying substrate display a variation in the observed intensities due to the phase difference in the beams after passing through the sample. The observed maxima in an XRR pattern correspond to situations where beams reflected off the thin film surface and ones reflected off the substrate are in phase. A number of these maxima, called Kiessig oscillations, can be seen in an XRR pattern, and it is possible to formulate a relationship between the thickness of the

film and the separation of the Kiessig oscillations, where the separations are inversely proportional to the film thickness.[84,85]

The XRR technique is particularly useful for the study of superlattices, i.e. periodic layered structures consisting of alternating layers of two different materials. The additional reflection, refraction and absorption of the incident X-ray beams at the interfaces of the different layers results in an XRR pattern where low-intensity oscillation peaks are flanked by high-intensity superlattice peaks. XRR patterns measured from thin films consisting of ZnO interspersed with single layers of hydroquinone are presented in Figure 3.

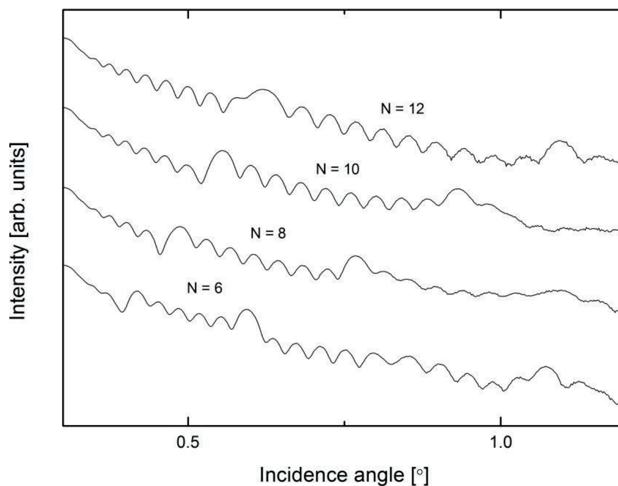

Figure 3 XRR patterns measured from thin films of ZnO:HQ superlattices. *N* stands for the number superlattice repetitions in the structure.

There is a strong correlation between the periodicity of the superlattice structure and the observed XRR pattern, as can be seen in Figure 3. Ideally, the number of smaller oscillations between the superlattice peaks would be equal to $N - 2$, where N is the number of superlattice repetitions in the film. In Figure 3, the observed peak counts match the expected numbers almost exactly, with only the N = 12 film showing a slight discrepancy in its pattern. The method works especially well for structures with relatively small N values, because signal noise that gets worse at higher incidence angles makes it difficult to count the exact number of oscillations for films with large numbers of superlattice layers.[85]

4.5 Optical Measurements

Optical reflectivity measurements were utilized to analyze the changes in carrier concentration in samples where it was high enough to be detectable with the technique, i.e. the Al- and P-doped ZnO films. The measurement setup used a light source in the infrared wavelength range corresponding to an energy range of 0.06 – 1.3 eV, which was shone at a normal angle on the sample surface. The measurement is based on the fact that the plasma frequency, ω_p, of a free electron gas can be seen in the reflectivity spectra of metals or doped semiconductors as a dip in reflectivity. The minimum point of this dip, called the Drude edge, determines the plasma frequency, which is proportional to the carrier concentration of the material according to the following equation based on the Drude-Lorentz model:

$$\omega_p = \left(\frac{ne^2}{m^* \varepsilon_\infty} \right)^{\frac{1}{2}} \quad (4)$$

where n is the charge carrier concentration, e is electron charge, m^* is the effective mass and ε_∞ is the high-frequency permittivity. Therefore, reflectivity measurements can be used as a relatively straightforward method to evaluate changes in carrier concentration when doping a semiconductor. An example of how changes in carrier concentration affect reflectivity measurements of Al-doped ZnO thin films is shown in Figure 4.

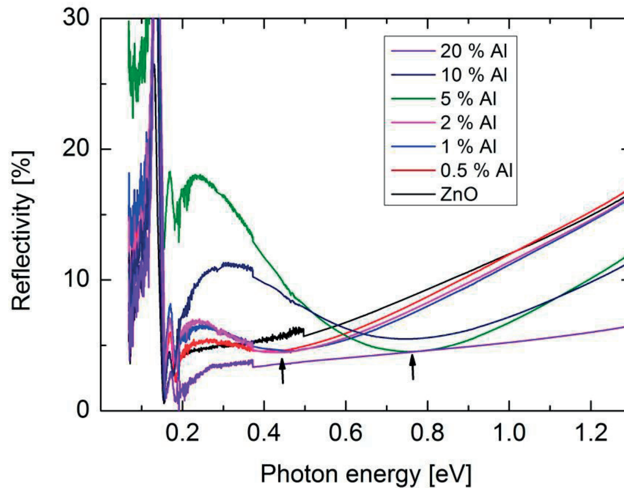

Figure 4 Reflectivity spectra for a series of Al-doped ZnO samples.[III]

The arrows in Figure 4 indicate the position of the Drude edge for selected measurements. It should be noted that the sharp drops in reflectivity

observed at around 0.15 - 0.2 eV in Figure 4 do not correspond to the Drude edge, but are instead caused by absorption of the incident light, most likely by the glass substrate of the thin films. The carrier concentration of the samples in Figure 4 can be seen to increase with increasing Al content, as indicated by the shift of the Drude edge towards higher energies. The doping reaches a limit at 5 at.% Al and at 20 at.% Al a clear reduction in the carrier concentration can be observed.

4.6 Thermoelectric Property Measurements

Measurements of the thermoelectric properties of the various ZnO films were performed using two homemade probes that were capable of measuring either the Seebeck coefficient or the resistivity at a temperature range of 5 – 300 K. The temperature control was performed by lowering the probes, which are at the ends of approximately 1 m long poles, into a tank of liquid helium and taking measurements every 0.5 – 2 degrees. The Seebeck coefficient was measured by using silver paste to attach the sample between two copper plates, one of which was thermally insulated from the rest of the probe, and applying a temperature gradient by heating the insulated Cu plate with a strain gauge heater. A thermometer was placed under the probe approximately at the sample position to measure the probe temperature, while a copper-constantan thermocouple was used to determine the hot-side temperature. Two different gradients (~0.5 and 1 degree) were applied and the Seebeck coefficient was calculated from the measured voltage and temperature difference. The resistivity measurement system was just an alumina sample mount with contacts for a four-point measurements and a thermometer underneath. Silver paste was again used for the contacts. Pictures of the measurement probes are provided in Figure 5.

Figure 5 Close-ups of the Seebeck coefficient (left) and resistivity (right) measurement probes.

Samples deposited on borosilicate glass were used for these measurements to minimize the influence of the substrate on the measurements. The effect of the various probe contacts and such on the Seebeck coefficient value was eliminated by using a superconducting sample and a piece of Cu wire to prepare a ground file, which was deducted from the measured values. Still, bad contacts sometimes caused a potentially large error on the Seebeck coefficient, so most measurements were repeated to ensure correct values. In the case of the resistivity measurements, X-ray reflectivity analysis was used to determine the thicknesses of the samples, and the width of the samples as well as the distance between contacts were measured with a digital caliper.

The uncertainty for the Seebeck coefficient measurement was determined by performing several measurements of samples cut from a single ZnO film on a borosilicate glass substrate and a standard deviation of 3.49 was obtained, corresponding to an error of 2.9 %. For resistivity measurements, the error in the measurement of the resistance of the sample was judged to be negligible compared to the uncertainty in measuring the dimensions of the sample, i.e. thickness, width and distance between contacts. The uncertainty in the thickness measurements was determined through repeated measurements and a variation of 0.01 mm was assumed for the digital caliper to obtain a total error of 3.6 %. When calculating the power factor based on the Seebeck coefficient and resistivity measurements these individual uncertainties result in the rather large error of 9.7 %.

5. Doping of ZnO Thin Films with Al and P

Aluminum doping of ZnO is a common method of improving the material's electrical properties, mainly for transparent conductor applications, and there are a large number of reports on ALD of Al-doped ZnO.[86-90] The objective of the previous studies, however, has been either to study the reaction mechanisms and chemistry involved or to decrease the resistivity of the films as much as possible. Al doping has been shown also to improve the thermoelectric properties of ZnO in bulk as well as thin film form, but there have not been any studies on the use of ALD in optimizing the thermoelectric performance of ZnO.

Phosphorus doping of ZnO has been studied mainly as a way to induce p-type conductivity in the material, which has been achieved through the use of numerous synthesis methods, including ALD.[91,92] However, the thermoelectric properties of P-doped ZnO have not been studied so far.

In this study, ALD was used to deposit films of Al- and P-doped ZnO thin films and the effect of the dopants on the thermoelectric properties of ZnO were investigated. The depositions were all performed on the R-100 ALD reactor using DEZ and H_2O as the ZnO precursors while trimethyl aluminum (TMA) and trimethyl phosphate (TMP) were used together with H_2O to deposit the doping layers of aluminum oxide and phosphorus oxide, respectively. Deposition temperatures were varied between 160 °C and 220 °C in order to elucidate the effect of deposition temperature on ZnO's transport properties.[II,III]

5.1 Chemical Composition and Structure

X-ray fluorescence and optical reflectivity measurements were performed to verify the incorporation of aluminum and phosphorus into the ZnO films. The XRF analysis showed the presence of the intended dopants in all the films, and there was a clear correlation between the XRF signals and the nominal concentration of the dopants. In the case of Al, especially at higher

dopant concentrations, there was more Al incorporated into the film than would be expected from the deposition program. This is due to a combination of two factors, namely the etching of existing ZnO film by the TMA precursor pulses as well as the fact that aluminum oxide layers have been observed to hinder the growth of the subsequent ZnO layers.[87] Therefore, the doping percentages discussed in this work signify the nominal dopant content rather than the exact amount present in the films.

Optical reflectivity measurements were used to evaluate the doping efficiency in a series of samples before performing more detailed transport property measurements. The reflectivity measurements for a series of Al- and P-doped ZnO films deposited at different temperatures are displayed in Figures 6 and 7. The appearance and shift to higher energies of the Drude edge is clearly visible in the reflectivity spectra for both dopants, although the effect is much more pronounced for P doping, indicating a higher degree of doping. The more subdued effect seen with Al doping at lower deposition temperatures could be a sign of less efficient doping, but the fact that ZnO itself, when deposited with ALD, has lower resistivity and hence higher carrier concentration at higher deposition temperatures likely plays a role here as well. Nonetheless, based on the reflectivity results, the emphasis of the transport property measurements of ZnO:Al films was placed on the films deposited at 220 °C due to the clearer doping effects. For P-doped ZnO, one of the objectives was to achieve p-type doping, so measurements were done mainly on the films deposited at 160 °C, where the intrinsic n-type doping of ZnO would be less significant.[II]

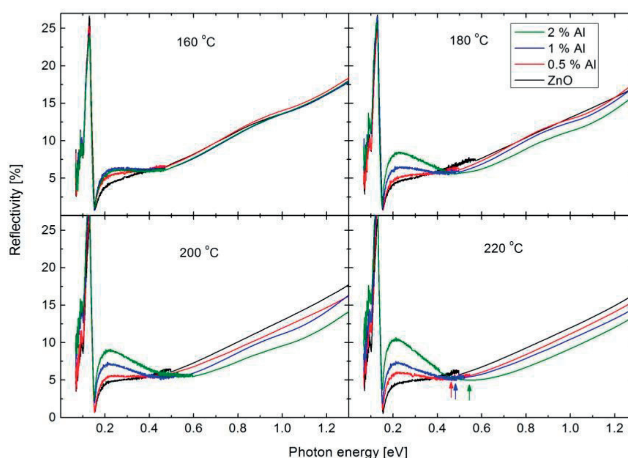

Figure 6 Reflectivity spectra for a series of Al-doped ZnO films.[II]

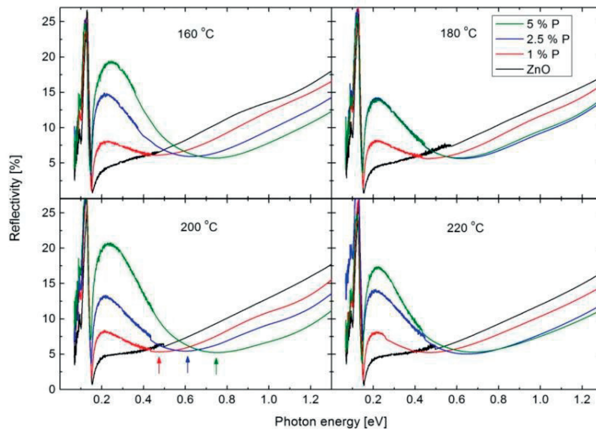

Figure 7 Reflectivity spectra for a series of P-doped ZnO films.[II]

GIXRD analysis of the doped film structures (Figure 8) revealed no changes in peak positions compared to pure ZnO, meaning that the lattice parameters were unchanged by the inclusion of dopants. There was, however, an effect on the relative intensities of the three main diffraction peaks of ZnO, i.e. the (100), (002) and (101) peaks. This could be a sign of increased grain orientation in the films, but one should not read too much into this, since the nature of the GIXRD measurement means that grain orientation cannot be reliably inferred from peak intensities, even though the change is systematic, especially in the case of P doping.[II]

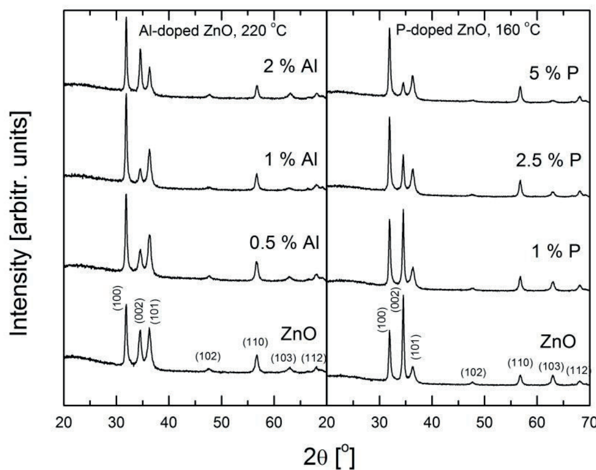

Figure 8 GIXRD patterns for doped ZnO showing variations in the diffraction intensities.[II]

5.2 Thermoelectric Properties

Both Al and P doping predictably resulted in the reduction of the Seebeck coefficient and resistivity values of ZnO as the carrier concentration was increased. Room-temperature values for both properties compared to the nominal dopant concentrations are presented in Figure 9. Both dopants are quite effective in increasing ZnO's carrier concentration with relatively large effect observed for low concentrations, followed by a more linear trend as the dopant concentration increases. The highest carrier concentrations for both Al and P were obtained at around 5 at.% doping, after which no further increase was observed, indicating that the solubility limit of the dopant into ZnO had been reached.[II]

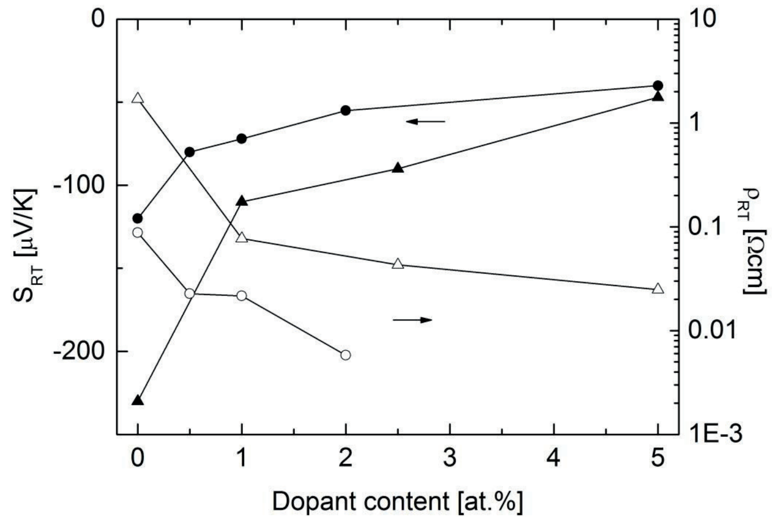

Figure 9 Room-temperature values for the Seebeck coefficient and resistivity of Al- and P-doped ZnO. Circles represent Al-doped ZnO deposited at 220 °C and triangles represent P-doped ZnO grown at 160 °C, while filled and empty symbols designate Seebeck coefficient and resistivity, respectively.

Using the values from Figure 9, the power factors for both dopants were calculated and are collected in Table 1. Aluminum was found to be more effective in improving the thermoelectric performance of ZnO with a high value of 0.052 mW/K^{2}m calculated for the film containing 2 % aluminum, compared to 0.016 mW/K^{2}m for the corresponding undoped ZnO film. P doping, on the other hand, reached a high of 0.019 mW/K^{2}m, although the corresponding ZnO film deposited at 160 °C only gave a power factor of 0.003 mW/K^{2}m. The improvement of the power factor with both dopants is based on the greatly reduced electrical resistivity that compensates for the

Table 1 Power factor values for Al- and P-doped ZnO films calculated from data in Figure 9.

Al doping [%]	Power factor [mW/K²m]	P doping [%]	Power factor [mW/K²m]
0	0.016	0	0.003
0.5	0.025	1	0.016
1	0.024	2.5	0.019
2	0.052	5	0.009

reduction in the Seebeck coefficient. Whether the doping would lead to an offsetting increase in thermal conductivity as well cannot be determined due to the difficulty of measuring thermal conductivity of thin films, but the significant increase observed in the power factor is very encouraging. The power factor values obtained for the Al-doped films are in the range typically reported for Al-doped ZnO thin films, although there is quite a lot of variation in the literature values owing to differences in deposition technique, deposition conditions and Al content, among other factors. Nevertheless, typical room-temperature values for the power factor of Al-doped ZnO films can be estimated to be 0.01-0.15 mW/K^2m, although values as high as 0.4 mW/K^2m have been reported.[51,61,93] There are no reports of the thermoelectric properties of P-doped ZnO to compare against, but the improvements observed in this work demonstrate that phosphorus is a viable dopant for the thermoelectric performance of ZnO.

An effort was also made to induce p-type conductivity in the P-doped ZnO films by subjecting the films to rapid thermal annealing (RTA) treatments for 10 minutes at a temperature range of 600-850 °C in air, as this has been reported to led to p-type conductivity in previous studies.[91,92] However, none of the treatments within this study was successful. All the RTA-treated ZnO:P samples resulted in films with extremely high resistivities, high enough that our Seebeck coefficient measurement system was unable to give any results at all. It is difficult to say for sure why the RTA-treatment did not work, but a strong possibility is that the annealing, even though it was only for a short time, caused the elimination of the intrinsic defects or impurities causing the high n-type carrier concentration of ZnO, resulting in a high resistivity value. This elimination of the n-type carriers should be necessary for achieving p-type conductivity, but the chemical species necessary for the generation of p-type carriers did not form in our ZnO:P films, and no p-type conductivity was observed.

6. ZnO-Organic Superlattice Structures

The combination of ALD and MLD has been used to fabricate a number of different hybrid inorganic-organic structures, and as the potential of these thin films for various applications is realized the number of studies on them is sure to increase dramatically. A variety of different organic precursors including ethylene glycol, nylon, hydroquinone, 4,4'-oxydianiline and several others have already been shown to be suitable for the deposition of hybrid thin films with ALD/MLD.[65-74] However, the emphasis in previous studies has been on the fabrication of hybrids with a 1:1 ratio of organic and inorganic layers or on so-called nanolaminates, where the ratios are varied to obtain thicker "blocks" of inorganic and hybrid layers stacked on top of each other. The ALD/MLD technique is also very well suited for the fabrication of hybrid superlattice structures, where single layers of the organic component are sandwiched between thicker layers of the inorganic component. These types of structures can have a huge effect on the material's thermoelectric properties, which has been demonstrated for inorganic superlattices,[25] but also predicted for hybrid superlattices.[75] Specifically, the fabrication of hybrid superlattices where the separation between organic layers is less than the mean free path of phonons (typically around 100 Å) would inhibit phonon transport and the consequent decrease in lattice thermal conductivity would improve the figure of merit of the material.

In this study, three different organic precursors were used in conjunction with the ZnO ALD process to fabricate hybrid superlattice films: hydroquinone (HQ), 4-aminophenol (AP) and 4,4'-oxydianiline (ODA). The precursors were chosen for their relatively simple structures and because of the expected rigidity of the benzene ring that is present in all the compounds. Hydroquinone can be described as a benzene ring with two –OH groups at opposite sides of the ring, while 4-aminophenol is identical except for an $-NH_2$ group replacing one of the –OH groups, and 4,4'-oxydianiline can be thought of as two 4-aminophenol rings joined at the

–OH group ends of the molecules. Illustrations of the organic precursors are presented in Figure 10.

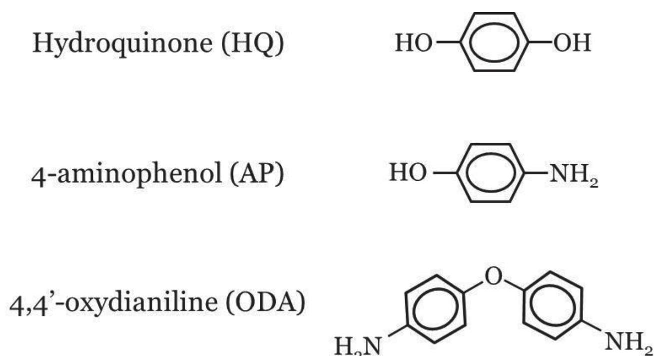

Figure 10 Chemical structures of the organic precursors used in the hybrid depositions.

The intention was that the –OH and $–NH_2$ groups at the ends of the molecules would react first with the Zn-OH surface and then the following DEZ pulse to form a distinct single organic layer within the ZnO film. The deposition temperature was fixed at 220 °C to obtain a higher conductivity for the ZnO phase and ZnO to organic layer ratios between 199:1 and 14:1 were deposited. The depositions were performed with the F-120 reactor and precursor temperatures for HQ, AP and ODA were 120 °C, 111 °C and 153 °C, respectively.[IV,VI]

6.1 Characterization of the Organic Layers

The fabrication of hybrid superlattice structures was successful with all the tested organic precursors, as was confirmed through XRR analysis. Figure 11 shows the XRR patterns of a number of ZnO:HQ thin films, where the characteristic peak patterns of superlattice structures are clearly visible. Moreover, considering that all depositions consisted of 600 ALD cycles, the number of smaller peaks visible between the superlattice peaks exactly matches the intended structure for ZnO:HQ ratios between 99:1 and 49:1. The presence of a superlattice is clear for the other ratios as well when compared to the pattern of pure ZnO, even though signal noise makes it impossible to count the number of peaks. ZnO:AP and ZnO:ODA films gave the same results, i.e. superlattice structures were evident in all samples and for the most part they matched the intended periodicity.[IV,VI]

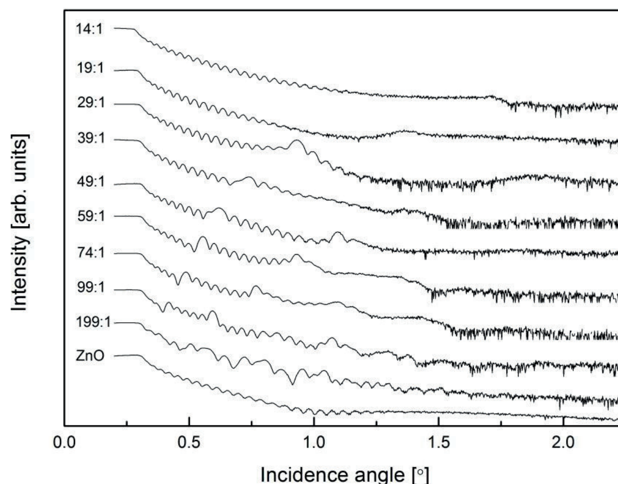

Figure 11 XRR patterns of ZnO:HQ thin films showing the presence of superlattice structures.[IV]

The XRR analysis could not tell anything about the nature of the superlattice layers, so to confirm that the organic precursors formed the intended layers FTIR spectroscopy was used. For this purpose, in order to increase the intensity of the organic absorption peaks, films with a 3:1 ZnO to organic ratio were prepared on Si substrates. The resulting FTIR patterns are presented in Figure 12.[VI]

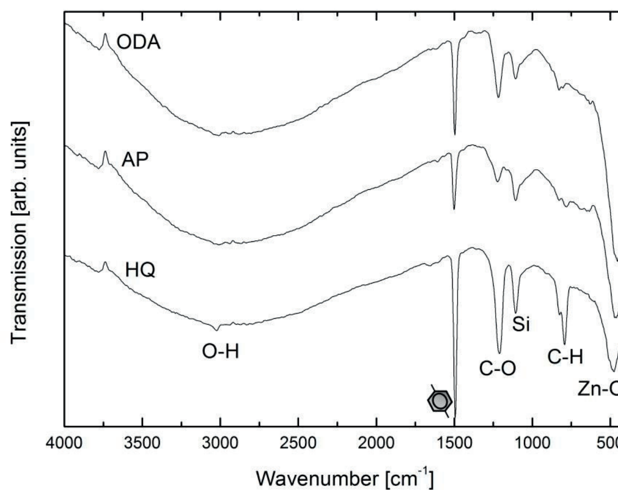

Figure 12 FTIR spectroscopy patterns of hybrid ZnO films with a 3:1 ZnO to organic ratio.[VI]

All the hybrid films show a similar FTIR pattern with a prominent benzene ring absorption peak at about 1500 cm^{-1} in addition to peaks from C-O, C-H and Zn-O bonds. The ZnO:HQ samples give by far the strongest absorption peaks, but all patterns clearly show the expected peaks. There is no sign of C-N or Zn-N peaks in the ZnO:AP and ZnO:ODA patterns, but these peaks would be expected to be found very close to the C-O and Zn-O peaks, so they could have merged together.

There is also a very wide absorption peak in all the patterns at around 2500 – 3500 cm^{-1}, which is typical of O-H bonds. This could come from atmospheric moisture reacting with the films or from the presence of unreacted –OH groups at the interface between the organic and inorganic layers. In fact, films with very high organic layer concentrations were found to be unstable in air, presumably reacting with atmospheric moisture. However, to avoid this, 20 additional layers of ZnO were deposited on top of the films made for FTIR analysis and the measurements were performed immediately after removal from the ALD reactor, so there would not seem to be enough time for significant amounts of atmospheric moisture to react with the films. Therefore, the O-H bonds are thought to be unreacted –OH groups at the inorganic-organic interfaces.

6.2 Thermoelectric Properties

The effect of the organic layers on the thermoelectric properties of ZnO was investigated at room temperature by measuring their Seebeck coefficients and resistivities. The obtained values are plotted in Figures 13 and 14. The effects from the organic layers all have the same trend, but their magnitude differs somewhat. All of them have a limited effect at low concentrations of organic layers and cause a small dip in the Seebeck coefficient and resistivity values before effecting a significant rise in both values. The observations are consistent with an initial rise in carrier concentration followed by a larger decrease. The most probable cause here is that the introduction of organic layers into the ZnO structure increases the number of impurities or vacancies in the ZnO lattice, thereby increasing the carrier concentration slightly. This effect would be offset at higher organic layer concentrations by the obvious hindrance caused to electron transport by the organic layers. More surprising is the large difference between the values of ZnO:HQ and ZnO:AP films, considering that the organic precursors differ by only one functional group.[VI]

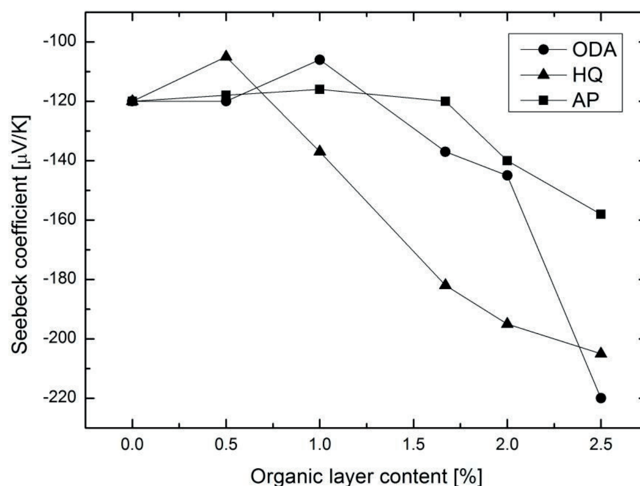

Figure 13 Room-temperature Seebeck coefficient values for the hybrid ZnO films.[VI]

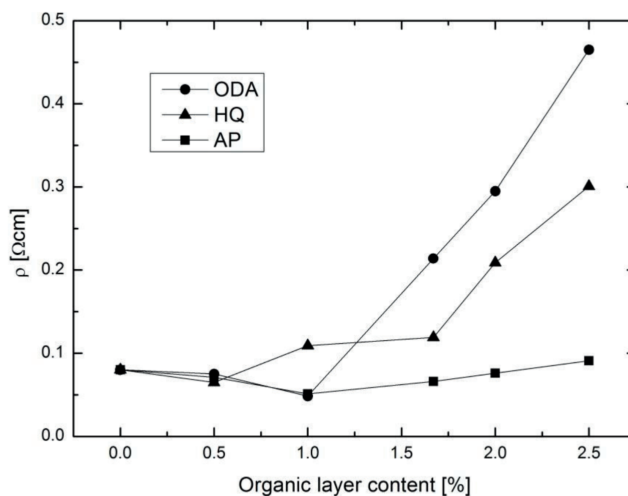

Figure 14 Room-temperature resistivity values for the hybrid ZnO films.[VI]

The effects of the organic layers on the power factor of ZnO varied depending on the precursor: AP resulted in an increasing trend, HQ gave relatively stable values, and ODA displayed a generally decreasing trend. However, these effects were quite small and the trends relatively unclear, so the main benefit from the organic layers is expected to come from a reduction in the material's thermal conductivity.

6.3 Hybrid Superlattices of Al-doped ZnO

In order to investigate the combined effects of organic layers and inorganic dopants on the thermoelectric properties of ZnO, a series of depositions was performed on the R-100 reactor where layers of hydroquinone and aluminum oxide were inserted into the ZnO film at fixed intervals. The deposition temperature was again 220 °C, and a precursor temperature of 160 °C was used for HQ. The chemical formula of the films could be described as $Zn_{1-2x}Al_xHQ_xO$, where *x* stands for the proportion of TMA/H_2O or HQ cycles out of the 600 ALD cycles deposited. An additional 5 cycles of ZnO were also deposited on top of the film as a capping layer to avoid any unforeseen effects from having an aluminum oxide layer at the very top of the film. As a result, the *x* values reported are slightly higher than the actual dopant layer proportions, but the error was not judged to be significant enough to warrant adjustment of the values in the following figures.[V]

Formation of the superlattice structure was observed from the organic layers as normal, as can be seen from the XRR patterns shown in Figure 15. The patterns look somewhat different from the ones in Figure 11, but the superlattice peak patterns are clearly visible and closely match the intended number of organic layers in the film. It is also noteworthy that the aluminum oxide layers did not cause the appearance of additional peaks in the superlattice peak patterns, as was expected from the assumption that Al would neatly fit into the ZnO lattice and thus would not cause a distinct layer to form in the structure.[V]

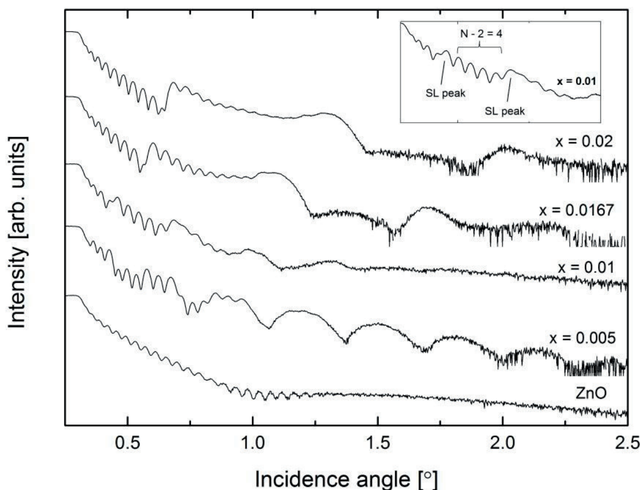

Figure 15 XRR patterns of a series of $Zn_{1-2x}Al_xHQ_xO$ films. The inset picture shows the determination of the number of superlattice repetitions, *N*, from the *x* = 0.01 sample.[V]

The stability of the organic layers at high temperatures was also tested by taking the $x = 0.01$ sample and heating it for 1 hour at a time at temperatures ranging from 300 °C to 700 °C and checking its XRR pattern for any changes. The resulting XRR patterns are pictured in Figure 16. The patterns show little change until the heating temperature reaches 500 °C, and even after 500 °C the superlattice peak patterns are still visible until 650 °C, although they are no longer as prominent as they were originally. Whether the organic layers are still present in their original state after heating at temperatures above 500 °C cannot be said from the XRR patterns alone, but judging from the nearly unchanged patterns obtained until 450 °C, it seems that the ZnO layers provide a significant improvement for the high-temperature stability of the hydroquinone layers, as they would be expected to burn in air at temperatures well below 450 °C.[V]

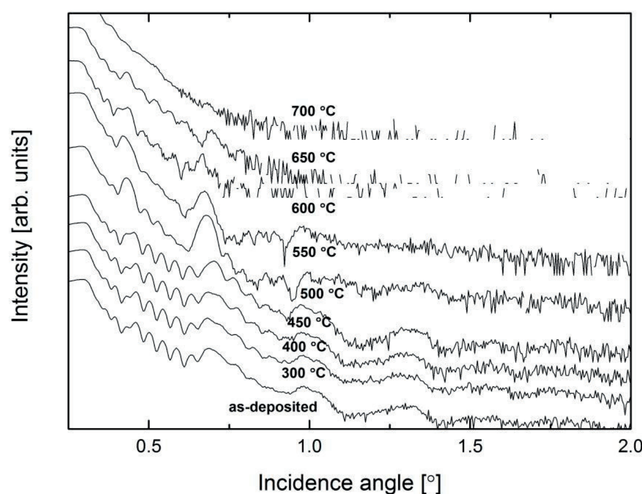

Figure 16 XRR patterns of the $x = 0.01$ sample after heating in air for one hour at a range of temperatures.[V]

The effects of the aluminum and hydroquinone layers on the thermoelectric properties of ZnO were investigated by measuring the films' Seebeck coefficient and resistivity values, which both showed a similar trend. The room-temperature values for both properties are shown in Figures 17 and 18. The combined effect of Al dopants and HQ layers results in Seebeck coefficient and resistivity values very close to those of Al-doped ZnO, with the organic layers causing an increase in both values only as x

reaches 0.02. In fact, the Seebeck values of the $Zn_{1-2x}Al_xHQ_xO$ films in Figure 17 are consistently slightly lower than with Al-doping alone, indicating a higher degree of carrier doping into the film.[V]

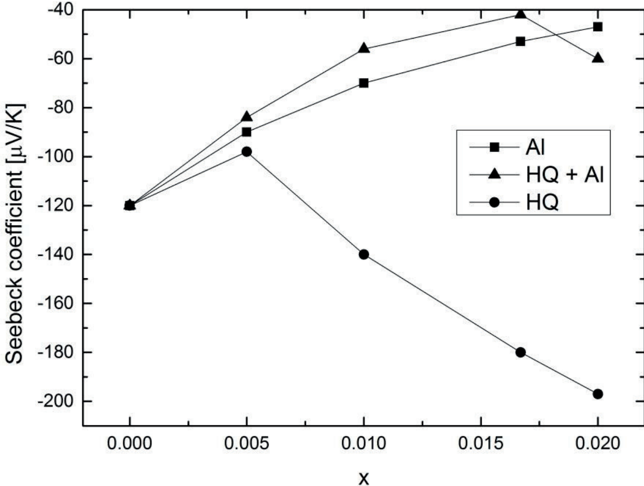

Figure 17 Room-temperature Seebeck coefficients for $Zn_{1-2x}Al_xHQ_xO$ films.[V]

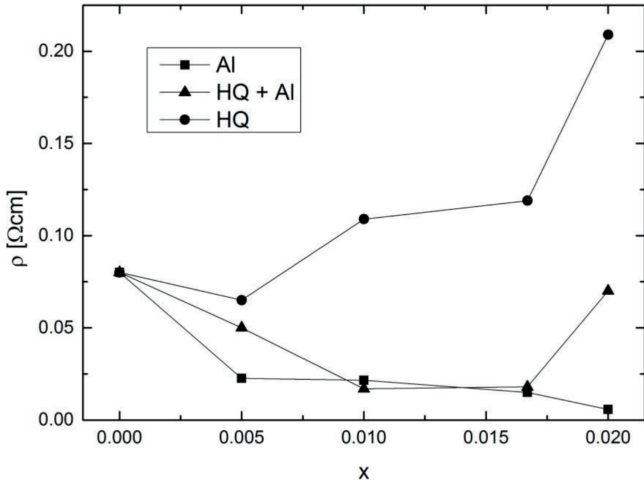

Figure 18 Resistivity values measured at room temperature for $Zn_{1-2x}Al_xHQ_xO$ films.

Using the data in Figures 17 and 18, the power factor was calculated for the $Zn_{1-2x}Al_xHQ_xO$ films (Table 2), and a generally decreasing trend was observed as *x* was increased. Therefore, the combination of Al doping and

Table 2 Power factor values calculated for the $Zn_{1-2x}Al_xHQ_xO$ films.

x	Power factor [mW/K²m]		
	Al	HQ	Al + HQ
0	0.018	0.018	0.018
0.005	0.028	0.015	0.014
0.01	0.022	0.018	0.018
0.0167	0.028	0.027	0.010
0.02	0.048	0.019	0.007

HQ layers does not result in a cumulative improvement in the power factor, but instead has a detrimental effect. Overall, the interplay of the organic layers and Al dopants was not as simple as was expected, and the tested range of compositions was relatively small, so there is a lot of room for improvement here. The data on the $Zn_{1-2x}Al_xHQ_xO$ films suggests that keeping the organic and Al dopant contents equal might not be ideal, and ZnO:HQ films with high concentrations of organic layers could benefit from a little Al doping.

Comparison of just the power factors would suggest that hydroquinone is not as effective as aluminum in improving the thermoelectric performance of ZnO, but this does not take into account the effect the organic layers have on the thermal conductivity of the material. This effect could be highly significant, because once x reaches 0.02 the separation between layers of HQ (about 49 layers of ZnO/aluminum oxide, or ~9-10 nm) reaches the scale where phonon transport is expected to be inhibited by the organic layers. The resulting decrease in lattice thermal conductivity would significantly improve the thermoelectric figure of merit of the hybrid materials. Inorganic superlattices of ZnO have been shown to cause a reduction in thermal conductivity of up to one magnitude,[46] and there is no reason why the organic layers would not result in equally great reductions. Unfortunately, due to the extremely challenging nature of reliably measuring the thermal conductivity of thin films, a reduction in thermal conductivity resulting from the organic layers could not be experimentally verified.

7. Conclusions

In this work, atomic layer deposition was used for the first time to study the effects of inorganic dopants as well as hybrid inorganic-organic superlattice structures on the thermoelectric properties of ZnO thin films. The inorganic dopants were observed to improve the power factor of ZnO in a predictable way, with Al turning out to be more effective in improving the thermoelectric performance of ZnO. The first successful fabrication of hybrid superlattice structures of ZnO was demonstrated with three different organic precursors, and all were found to have a similar, slightly non-linear effect on the thermoelectric properties of ZnO. The combination of Al doping and hybrid superlattice layers, however, did not result in a cumulative improvement in the power factor of ZnO, resulting instead in somewhat decreased performance. Still, there is a lot of promise in combining inorganic dopants and organic layers to improve the thermoelectric performance of ZnO, as there is a great variety of dopant substances and amounts that could lead to a positive effect on the power factor. Moreover, considering the strong possibility that the organic layers will cause a reduction in the lattice thermal conductivity of ZnO films, appropriately spaced hybrid superlattices might be by themselves enough to bring about a significant improvement in the figure of merit of ZnO.

The fabrication of the hybrid superlattice structures is also interesting from a theoretical viewpoint, as these types of structures have been researched very little so far. The observed non-linear effects on the transport properties of ZnO could be the result of the organic precursors affecting the impurities or defects causing ZnO's unique intrinsic carrier doping. Perhaps the organic precursors do not form a complete layer or hinder the growth of subsequent ZnO layers with the result of additional defects that cause the observed slight increase in carrier concentration, which is then offset at higher concentrations by the increased hindrance to electron movement. Further study will be required to fully elucidate the interaction of the inorganic and organic phases in hybrid superlattice structures.

The priority for further studies on the thermoelectric properties of hybrid thin films should be in determining the effect of the organic layers on the thermal conductivity of the films. If the anticipated phonon hindering effect is real, there could be significant improvements in the figure of merit of ZnO, and this would have implications for the nanostructuring of other thermoelectric materials as well, since there is no reason why the organic layers would not have the same effect on a number of other materials. A wealth of different organic molecules and their combinations with various inorganic dopants remain to be investigated in this regard, and hybrid materials could end up having a large contribution to the field of thermoelectric materials research.

References

1. K. Salzgeber, P. Prenninger, A. Grytsiv, P. Rogl and E. Bauer, *J. Electron. Mater.* **39** (2009) 2074-2078.
2. H. Kleinke, *Chem. Mater.* **22** (2010) 604-611.
3. I. Terasaki, *Physica B* **328** (2003) 63-67.
4. J. He, Y. Liu and R. Funahashi, *J. Mater. Res.* **26** (2011) 1762-1772.
5. L. D. Hicks and M. S. Dresselhaus, *Phys. Rev. B* **47** (1993) 12727-12731.
6. G. J. Snyder and E. S. Toberer, *Nature Mater.* **7** (2008) 105-114.
7. A. J. Minnich, M. S. Dresselhaus, Z. F. Ren and G. Chen, *Energy Environ. Sci.* **2** (2009) 466-479.
8. C. J. Vineis, A. Shakouri, A. Majumdar and M. G. Kanatzidis, *Adv. Mater.* **22** (2010) 3970-3980.
9. K. Nielsch, J. Bachmann, J. Kimling and H. Böttner, *Adv. Energy Mater.* **1** (2011) 713-731.
10. Z. H. Dughaish, *Physica B* **322** (2002) 205-223.
11. A. D. LaLonde, Y. Pei, H. Wang and G. J. Snyder, *Mater. Today* **14** (2011) 526-532.
12. H. Ohta, K. Sugiura and K. Koumoto, *Inorg. Chem.* **47** (2008) 8429-8436.
13. M. Ohtaki, T. Tsubota, K. Eguchi and H. Arai, *J. Appl. Phys.* **79** (1996) 1816-1818.
14. T. Tsubota, M. Ohtaki, K. Eguchi and H. Arai, *J. Mater. Chem.* **7** (1997) 85-90.
15. M. Ohtaki, K. Araki and K. Yamamoto, *J. Electron. Mater.* **38** (2009) 1234-1238.
16. M. Knez, K. Nielsch and L. Niinistö, *Adv. Mater.* **19** (2007) 3425-3438.
17. H. Kim, H.-B.-R. Lee and W.-J. Maeng, *Thin Solid Films* **517** (2009) 2563-2580.
18. S. M. George, B. Yoon and A. A. Dameron, *Acc. Chem. Res.* **42** (2009) 498-508.
19. T. M. Tritt, *Annu. Rev. Mater. Res.* **41** (2011) 433-448.
20. J. R. Sootsman, D. Y. Chung and M. G. Kanatzidis, *Angew. Chem. Int. Ed.* **48** (2009) 8616-8639.

21. G. Joshi, H. Lee, Y. Lan, X. Wang, G. Zhu, D. Wang, R. W. Gould, D. C. Cuff, M. Y. Tang, M. S. Dresselhaus, G. Chen and Z. Ren, *Nano Lett.* **8** (2008) 4670-4674.
22. B. Poudel, Q. Hao, Y. Ma, Y. Lan, A. Minnich, B. Yu, X. Yan, D. Wang, A. Muto, D. Vashaee, X. Chen, J. Liu, M. S. Dresselhaus, G. Chen and Z. Ren, *Science* **320** (2008) 634-638.
23. M. S. Dresselhaus, G. Chen, Z. F. Ren, G. Dresselhaus, A. Henry and J.-P. Fleurial, *JOM* **61** (2009) 86-90.
24. T. C. Harman, P. J. Taylor, D. L. Spears and M. P. Walsh, *J. Electron. Mater.* **29** (2000) L1.
25. R. Venkatasubramanian, E. Siivola, T. Colpitts and B. O'Quinn, *Nature* **413** (2001) 597-602.
26. R. Y. Wang, J. P. Feser, J.-S. Lee, D. V. Talapin, R. Segalman and A. Majumdar, *Nano Lett.* **8** (2008) 2283-2288.
27. J. O. Sofo and G. D. Mahan, *Appl. Phys. Lett.* **65** (1994) 2690-2692.
28. D. A. Broido and T. L. Reinecke, *Phys. Rev. B* **51** (1995) 13797-13800.
29. L. D. Hicks, T. C. Harman, X. Sun and M. S. Dresselhaus, *Phys. Rev. B* **53** (1996) 493-496.
30. M. S. Dresselhaus, G. Chen, M. Y. Tang, R. Yang, H. Lee, D. Wang, Z. Ren, J.-P. Fleurial and P. Gogna, *Adv. Mater.* **19** (2007) 1043-1053.
31. G. Chen, *Phys. Rev. B* **57** (1998) 14958-14973.
32. R. Vankatasubramanian, *Phys. Rev. B* **61** (2000) 3091-3097.
33. V. A. Coleman and C. Jagadish, *Zinc Oxide Bulk, Thin Films and Nanostructures*, ed C. Jagadish and S. J. Pearton (2006) Elsevier, Amsterdam, p 1-20.
34. A. Janotti and C. G. Van de Walle, *Rep. Prog. Phys.* **72** (2009) 126501.
35. V. A. Karpina, V. I. Lazorenko, C. V. Lashkarev, V. D. Dobrowolski, L. I. Kopylova, V. A. Baturin, S. A. Pustovoytov, A. J. Karpenko, S. A. Eremin, P. M. Lytvyn, V. P. Ovsyannikov and E. A. Mazurenko, *Cryst. Res. Technol.* **39** (2004) 980-992.
36. A. F. Kohan, G. Ceder, D. Morgan and C. G. Van de Walle, *Phys. Rev. B* **61** (2000) 15019-15027.
37. C. G. Van de Walle, *Physica B* **308-310** (2001) 899-903.
38. A. Janotti and C. G. Van de Walle, *J. Cryst. Growth* **287** (2006) 58-65.
39. K. Minegishi, Y. Koiwai, Y. Kikuchi, K. Yano, M. Kasuga and A. Shimizu, *Jpn. J. Appl. Phys.* **36** (1997) L1453-455.

40. D. C. Looks, D. C. Reynolds, C. W. Litton, R. L. Jones, D. B. Eason and G. Cantwell, *Appl. Phys. Lett.* **81** (2002) 1830-1832.
41. K.-K. Kim, H.-S. Kim, D.-K. Hwang, J.-H. Lim and S.-J. Park, *Appl. Phys. Lett.* **83** (2003) 63-65.
42. M. Ohtaki, D. Ogura, K. Eguchi and H. Arai, *J. Mater. Chem.* **4** (1994) 653-656.
43. H. Ohta, W.-S. Jeon and K. Koumoto, *J. Am. Ceram. Soc.* **79** (1996) 2193-2196.
44. Y. Masuda, M. Ohta, W.-S. Seo, W. Pitschke and K. Koumoto, *J. Solid State Chem.* **150** (2000) 221-227.
45. T. Tani, S. Isobe, W.-S. Seo and K. Koumoto, *J. Mater. Chem.* **11** (2001) 2324-2328.
46. X. Liang, M. Baram and D. R. Clarke, *Appl. Phys. Lett.* **102** (2013) 223903.
47. P. Jood, R. J. Mehta, Y. Zhang, G. Peleckis, X. Wang, R. W. Siegel, T. Borca-Tasciuc, S. X. Dou and G. Ramanath, *Nano Lett.* **11** (2011) 4337-4342.
48. J. Aranovich, A. Ortiz and R. H. Bube, *J. Vac. Sci. Technol.* **16** (1979) 994-1003.
49. L. Li, L. Fang, K. J. Liao, G. Z. Fu, F. F. Yang, G. B. Liu, R. J. Zhang, C. L. Cao and W. M. Chen, *J. Cryst. Growth* **287** (2006) 101-104.
50. L. Li, L. Fang, X. M. Chen, J. Liu, F. F. Yang, Q. J. Li, G. B. Liu and S. J. Feng, *Physica E* **41** (2008) 169-174.
51. N. Vogel-Schäuble, Y. E. Romanyuk, S. Yoon, K. J. Saji, S. Populoh, S. Pokrant, M. H. Aguirre and A. Weidenkaff, *Thin Solid Films* **520** (2012) 6869-6875.
52. A. I. Abutaha, S. R. Sarath Kumar and H. N. Alshareef, *Appl. Phys. Lett.* **102** (2013) 053507.
53. A. Sarkar, S. Ghosh, S. Chaudhuri and A. K. Pal, *Thin Solid Films* **204** (1991) 255-264.
54. Y. Orikasa, N. Hayashi and S. Muranaka, *J. Appl. Phys.* **103** (2008) 113703.
55. L. Fang, X. F. Yang, L. P. Peng, K. Zhou, F. Wu, Q. L. Huang and C. Y. Kong, *J. Supercond. Nov. Magn.* **23** (2010) 889-892.
56. G. K. Paul and S. K. Sen, *Mater. Lett.* **57** (2002) 742-746.
57. F. Wu, L. Fang, Y. J. Pan, K. Zhou, L. P. Peng, Q. L. Huang and C. Y. Kong, *Appl. Surf. Sci.* **255** (2009) 8855-8859.
58. A. Z. Barasheed, S. R. Sarath Kumar and H. N. Alshareef, *J. Mater. Chem. C* **1** (2013) 4122-4127.
59. D. K. Seo, B. H. Kong and H. K. Cho, *Cryst. Growth Des.* **10** (2010) 4638-4641.

60. D. K. Seo, S. Shin, H. H. Cho, B. H. Kong, D. M. Whang and H. K. Cho, *Acta Mater.* **59** (2011) 6743-6750.
61. S. Teehan, H. Efstathiadis and P. Haldar, *J. Alloys Compd.* **509** (2011) 1094-1098.
62. J. H. Kim, D. K. Seo, C. H. Ahn, S. W. Shin, H. H. Cho and H. K. Cho, *J. Mater. Chem.* **22** (2012) 16312.
63. N. Vogel-Schäuble, T. Jaeger, Y. E. Romanyuk, S. Populoh, C. Mix, G. Jakob and A. Weidenkaff, *Phys. Status Solidi RRL* **7** (2013) 364-367.
64. G. Homm, F. Gather, A. Kronenberger, S. Petznick, T. Henning, M. Eickhoff, B. K. Meyer, C. Heiliger and P. J. Klar, *Phys. Status Solidi A* **210** (2013) 119-124.
65. S. George, A. Dameron, Y. Du, N. M. Adamczyk and S. Davidson, *ECS Trans.* **11** (2007) 81-90.
66. B. H. Lee, M. K. Ryu, S.-Y. Choi, K.-H. Lee, S. Im and M. M. Sung, *J. Am. Chem. Soc.* **129** (2007) 16034-16041.
67. O. Nilsen, K. B. Klepper, H. Ø. Nielsen and H. Fjellvåg, *ECS Trans.* **16** (2008) 3-14.
68. A. A. Dameron, D. Seghete, B. B. Burton, S. D. Davidson, A. S. Cavanagh, J. A. Bertrand and S. M. George, *Chem. Mater.* **20** (2008) 3315-3326.
69. B. Yoon, D. Seghete, A. S. Cavanagh and S. M. George, *Chem. Mater.* **21** (2009) 5365-5374.
70. Q. Peng, B. Gong, R. M. VanGundy and G. N. Parsons, *Chem. Mater.* **21** (2009) 820-830.
71. A. Sood, P. Sundberg, J. Malm and M. Karppinen, *Appl. Surf. Sci.* **257** (2011) 6435-6439.
72. K.-H. Yoon, K.-S. Han and M.-M. Sung, *Nanoscale Res. Lett.* **7** (2012) 71.
73. B. Yoon, B. H. Lee and S. M. George, *J. Phys. Chem. C* **116** (2012) 24784-24791.
74. A. Sood, P. Sundberg and M. Karppinen, *Dalton Trans.* **42** (2013) 3869-3875.
75. J. Carrete, N. Mingo, G. Tian, H. Ågren, A. Baev and P. N. Prasad, *J. Phys. Chem. C* **116** (2012) 10881-10886.
76. E. Guziewicz, M. Godlewski, T. Krajewski, Ł Wachnicki, A. Szczepanik, K. Kopalko, A. Wójcik-Głodowska, E. Przeździecka, W. Paszkowicz, E. Łusakowska, P. Kruszewski, N. Huby, G. Tallarida and S. Ferrari, *J. Appl. Phys.* **105** (2009) 122413.
77. E. B. Yousfi, J. Fouache and D. Lincot, *Appl. Surf. Sci.* **153** (2000) 223-234.

78. P.-Y. Lin, J.-R. Gong, P.-C. Li, T.-Y. Lin, D.-Y. Lyu, D.-Y. Lin, H.-J. Lin, T.-C. Li, K.-J. Chang and W.-J. Lin, *J. Cryst. Growth* **310** (2008) 3024-3028.
79. J. T. Tanskanen, J. R. Bakke, T. A. Pakkanen and S. F. Bent, *J. Vac. Sci. Technol. A* **29** (2011) 031507.
80. S.-Y. Pung, K.-L. Choy, X. Hou and C. Shan, *Nanotechnol.* **19** (2008) 435609.
81. J. Malm, E. Sahramo, J. Perälä, T. Sajavaara and M. Karppinen, *Thin Solid Films* **519** (2011) 5319-5322.
82. N. Y. Yuan, S. Y. Wang, C. B. Tan, X. Q. Wang, G. G. Chen and J. N. Ding, *J. Cryst. Growth* **366** (2013) 43-46.
83. J.-E. Kim, S.-M. Bae, H. Yang and J.-H. Hwang, *J. Korean Ceram. Soc.* **47** (2010) 353-356.
84. H. Kiessig, *Ann. Phys.* **10** (1931) 769.
85. M. Birkholz, *Thin Film Analysis by X-Ray Scattering* (2006) Wiley-VCH, Weinheim, p. 165-175.
86. V. Lujala, J. Skarp, M. Tammenmaa and T. Suntola, *Appl. Surf. Sci.* **82/83** (1994) 34-40.
87. J. W. Elam, Z. A. Sechrist and S. M. George, *Thin Solid Films* **414** (2002) 43-55.
88. S. J. Kwon, *Jpn. J. Appl. Phys.* **44** (2005) 1062-1066.
89. J.-S. Na, Q. Peng, G. Scarel and G. N. Parsons, *Chem. Mater.* **21** (2009) 5585-5593.
90. P. Banerjee, W.-J. Lee, K.-R. Bae, S. B. Lee and G. W. Rubloff, *J. Appl. Phys.* **108** (2010) 043504.
91. H. Yuan, B. Luo, S. A. Campbell and W. L. Gladfelter, *Electrochem. Solid-State Lett.* **14** (2011) H181-H183.
92. Y. T. Shih, J. F. Chien, M. J. Chen, J. R. Yang and M. Shiojiri, *J. Electrochem. Soc.* **158** (2011) H516-H520.
93. P. Mele, S. Saini, H. Honda, K. Matsumoto, K. Miyazaki, H. Hagino and A. Ichinose, *Appl. Phys. Lett.* **102** (2013) 253903.

Aalto-DD 194/2013

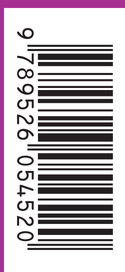

ISBN 978-952-60-5452-0
ISBN 978-952-60-5453-7 (pdf)
ISSN-L 1799-4934
ISSN 1799-4934
ISSN 1799-4942 (pdf)

Aalto University
School of Chemical Technology
Department of Chemistry
www.aalto.fi

BUSINESS +
ECONOMY

ART +
DESIGN +
ARCHITECTURE

SCIENCE +
TECHNOLOGY

CROSSOVER

DOCTORAL
DISSERTATIONS